Identification of macrophage/microglia activation factor (MAF) associated with late endosomes/lysosomes in microglial cells

Anja U. Bräuer, Robert Nitsch, Nicolai E. Savaskan*

Institute of Cell Biology and Neurobiology, Center for Anatomy, Charité University Medical School Berlin, Philippstr. 12, D-10115 Berlin, Germany

Received 3 January 2004; revised 20 February 2004; accepted 25 February 2004

First published online 11 March 2004

Edited by Lukas Huber

Abstract Damage to the central nervous system triggers rapid activation and specific migration of glial cells towards the lesion site. There, glial cells contribute heavily to secondary neuronal changes that take place after lesion. In an attempt to identify the molecular cues of glial activation following brain trauma we performed differential display reverse transcription-polymerase chain reaction screenings from lesioned and control hippocampus. Here we report on the identification of the macrophage/microglia activation factor (MAF), a new membrane protein with seven putative transmembrane domains. Expression analysis revealed that MAF is predominantly expressed in microglial cells in the brain, and is upregulated following brain lesion. Overexpression of MAF in non-glial cells shows an intracellular codistribution with the lysosomal marker endosome/lysosome-associated membrane protein-1 (lamp-1). Furthermore, MAF-transfected cells show that MAF is primarily associated with late endosomes/lysosomes, and that this association can be disrupted by activation of protein kinase C-dependent pathways. In conclusion, these results imply that MAF is involved in the dynamics of lysosomal membranes associated with microglial activation following brain lesion.

Key words: Lamp-1; Hippocampal lesion; Late endosome/lysosome; Phagocytosis; PKC signal transduction

1. Introduction

Brain damage, such as stroke and trauma, induces substantial remodeling of neuronal structures and connectivity [1–3]. Such remodeling is driven by endogenous neuronal programs reinitiating embryonic growth feasibility as well as by glial activation responses [4,5]. A well-characterized system for analyzing these phenomena is the entorhino-hippocampal lesion model [6]. Axons from the entorhinal cortex terminate in a laminar-specific fashion in the hippocampus. Furthermore, this particular axonal projection is severely altered in neurodegenerative conditions such as Alzheimer's disease, leading to microglial activation, axonal degeneration, and disconnection of the limbic structure [7–9]. Microglia are cells of the monocyte/macrophage lineage naturally populating the brain parenchyma [10]. There, they exist in two major functional states: non-activated (ramified, or resting) and activated (ameboid). Lesioning the entorhinal cortex induces a rapid activation and migration of microglial cells to the site of the injury, a feature also found in neurodegenerative diseases [11,12]. This activation induces an ameboid-like phenotype in microglial cells which is associated with enhanced phagocytotic activity, the expression of various immunomodulatory factors, and the secretion of inflammatory and cytotoxic molecules leading to secondary neuronal damage [2,13,14].

In an attempt to identify which molecules are associated with the activation of microglial cells and secondary damage to neurons, we performed a differential display screening with cDNAs obtained from lesioned hippocampi [15]. Here we report on the identification of a new macrophage/microglia activation factor (MAF). MAF is expressed by microglial cells following activation. Expression analysis revealed that MAF is predominantly expressed in the brain. Thus, we identified a membrane protein with seven putative transmembrane domains specifically expressed by microglial cells. We also show that MAF is associated with endosome/lysosome-associated membrane protein-1 (lamp-1) positive late endosomes/lysosomes and its expression is upregulated following lesion. Furthermore, MAF-associated vesicular structures are secreted in a protein kinase C (PKC)-dependent manner. Our data suggest that activated microglial cells have a neurotoxic role which may contribute to secondary neuronal degeneration following brain lesion.

2. Materials and methods

2.1. Animal manipulation and tissue isolation

Adult male Sprague rats (200–250 g weight) obtained from our central animal facility (Tierexperimentelle Einrichtung Charité, Dr. S. Nagel) were kept under standard laboratory conditions in accordance with the German and European Guidelines for the use of laboratory animals (in congruence with 86/609/EEC). All surgical procedures were performed in agreement with the German law on the use of laboratory animals. For stereotactic surgery, rats were anesthetized with a mixture of 25 mg/ml ketamine (CuraMed Pharma GmbH, Karlsruhe, Germany), 1.2 mg/ml xylazine (Bayer, Leverkusen, Germany) and 0.35 mg/ml acepromazine (Sanofi GmbH, Düsseldorf, Germany) in 0.9% sterile NaCl (2.5 ml/kg body weight intraperitoneally (i.p.)) and received a unilateral entorhinal cortex lesion (ECL) through the use of a stereotaxic headholder (Stoelting, Germany) [15]. In brief, a standard electrocoagulator was used to make bilateral incisions (with four single pulses (2.5 μA) for 3 s each) in the frontal and sagittal planes between the entorhinal cortex and hippocampus. The following coordinates measured from lambda were used: frontal incision: AP +1.2, L 3.1 to 6.1, and V down to the inferior cranium; sagittal incision: AP +1.2 to +4.2, L 6.1, and V down to the inferior cranium [16]. Rats were allowed to survive for 1 and 10 days ($n = 4$ animals per stage for in situ hybridization; $n = 6$ animals at 1 day after

*Corresponding author. Fax: (49)-30-450 528 902. Present address: The Netherlands Cancer Institute, Division of Cellular Biochemistry, Plesmanlaan 121, 1066 CX Amsterdam, The Netherlands.
E-mail address: nicolai.savaskan@charite.de (N.E. Savaskan).

0014-5793/04/$30.00
doi:10.1016/S0014-5793(04)00244-3

lesion (dal) for differential display reverse transcription-polymerase chain reaction (DDRT-PCR) and Northern blot analysis). The rats were decapitated under deep ether anesthesia (Chinosol, Germany).

2.2. Differential mRNA display and molecular cloning

For DDRT-PCR, the hippocampi of six lesioned (1 dal stage) and six untreated control animals were rapidly removed and washed in 0.1 M phosphate buffer and subsequently frozen in liquid nitrogen. Total RNA was extracted from the hippocampi using the guanidinium thiocyanate-phenol-chloroform extraction method [17]. DNA-free RNA was obtained by treatment with RNase-free DNase I (Boehringer, Germany) for 30 min at 37°C. After phenol-chloroform extraction and ethanol precipitation, the probes were stored at −80°C. The first strand reactions contained 50 ng oligo(dt_{11}-NN), 400 units of superscript II RT$^-$ transcriptase and 100 nM dithiothreitol (DTT) in 20 μl 1×transcription buffer (all from Gibco, Germany) and were incubated with 2 μg RNA and 200 μM deoxyribonucleoside triphosphate (dNTP) (Pharmacia Biotech, Germany) for 1 h at 42°C. Following first strand synthesis, two units of RNase H$^-$ (Gibco, Germany) were added and the reactions were incubated at 37°C for 30 min. The cDNA was purified using the PCR purification kit (Qiagen, Germany). PCR was performed using 2 μl of the RT reaction per 25 μl. All reactions were performed in quadruples. Anchor and arbitrary primers (Roth, Germany) were used in different combinations. Reactions were performed in 25 mM $MgCl_2$, 2.5 μl 10×reaction buffer, 2.5 units Amplitaq Gold (all from Perkin Elmer, USA), 200 mM dNTP (Pharmacia Biotech, Germany), 20 pmol per anchor primer and 10 pmol per arbitrary primer. The cycler program was: 95°C, 10 min; 40°C, 90 s; 72°C, 45 s followed by 39×(94°C, 30 s; 40°C, 90 s; 72°C, 45 s); 5 min at 72°C, and then soaked at 4°C. For electrophoretic separation, the entire PCR reaction was precipitated with ethanol. For the analysis of the PCR products, the CleanGel DNA analysis kit and the DNA silver staining kit (both from Pharmacia Biotech, Germany) were used according to the manufacturer's instructions. Those bands differing in expression between lesioned and control animals were excised and reamplified in 25 μl reaction using the same conditions as before. The resulting fragments were cloned into the pCR®2.1-TOPO Vector (Invitrogen, The Netherlands) and sequenced. MAF full-length clones were amplified by RT-PCR from postnatal and adult rat and mouse hippocampus cDNA and human hemapoetic cell lines. Database searches used BLAST on the website of the National Center for Biotechnology Information (NCBI). Multiple sequence alignments were made with Clustal W using the DNAsis Max v1.1 software (Hitachi, Olivet Cedex, France). Transmembrane structures were predicted with ProDom, PREDICT PROTEIN, TMPRED, and SwissProt databases. The rat MAF sequence is deposited at the NCBI homepage (GenBank accession number AF540876). The MAF open reading frame was further tagged with enhanced green fluorescent protein (eGFP) at the N-terminus and at the C-terminus and cloned into a pcDNA 3.1 based vector (Invitrogen, Germany). Both, N-terminal tagged MAF as well as C-terminal tagged MAF showed essentially the same subcellular distribution.

2.3. Northern blot analysis

The isolation of RNA from brains was performed as described under Section 2.2. Messenger RNA from cell lines was isolated with MidiMACS mRNA isolation columns (Miltenyi Biotec, Bergisch Gladbach, Germany). A total of 20 μg of RNA from six adult control and six 1 dal animals was loaded on a 1% agarose gel containing formaldehyde, transferred to Hybond™-N membrane (Amersham Life Science, UK) and crosslinked by ultraviolet irradiation. As a probe for MAF, the 1240 bp differential display fragment was used. A cDNA β-actin fragment amplified by RT-PCR served as a control for mRNA integrity and amounts of mRNA loaded. Primers for the amplification of the control gene β-actin were: β-actin 5′ (5′-CAC CAC AGC TGA GAG GGA AAT CGT GCG TGA-3′) spanning bases 2395–2424, and β-actin 3′ (5′-ATT TGC GGT GCA GCA TGG AGG GGC CGG ACT-3′) complementary to bases 3095–3124, with an amplification length of 520 bp for rat β-actin cDNA (GenBank accession number J00691). PCR was performed in 25 μl final volume containing 1 mM dNTP (Pharmacia Biotech, Germany), 2.5 units Taq polymerase (Perkin Elmer, USA), 2.5 μl 10×buffer including 2.5 M $MgCl_2$ (Perkin Elmer, USA), 10 μM of each primer, and 1 μl cDNA using a Thermo-Cycler PTC-100 (MJ Research, Inc., USA). The cycle program was: 95°C, 2 min; 35×(94°C, 30 s; 70°C, 30 s; 72°C, 2 min); and 72°C, 10 min. Both probes were labeled with the Prime-a-Gene Labeling System (Promega, USA) and [^{32}P]dCTP (DuPont NEN, USA). Hybridization was performed in 10 ml hybridization solution (250 mM sodium phosphate, pH 7.2, 7% sodium dodecyl sulfate (SDS), 0.5 mM ethylenediamine tetraacetic acid (EDTA), 1% bovine serum albumin (BSA)) at 60°C for 12 h. The membrane was washed in 2×standard sodium citrate (SSC) at room temperature, 0.2×SSC at room temperature, and 0.2×SSC at 40°C for 30 min each. Membranes were exposed to Kodak X-OMAT AR X-ray films at −80°C for 20 h, using an intensifying screen.

2.4. In situ hybridization

For in situ hybridization experiments, four brains per lesion stage were dissected and frozen in the gaseous phase of liquid nitrogen. Horizontal cryostat sections (15 μm) were fixed in 4% paraformaldehyde (w/v), washed in 0.1 M phosphate buffer saline (PBS, pH 7.4) and dehydrated. For in situ hybridization the following oligonucleotides were used: antisense oligonucleotides 5′-CAT GAG CCA GAT AAA CCA ACG CAT ATG AGA TGC CAG-3′ and 5′-ACA ATG GCC CGA ACA ATG AGG AAT GCG TGT GTG TAG C-3′ complementary to rat and mouse MAF mRNA (GenBank accession number AF540876) and their sense oligonucleotides. Both oligonucleotides gave essentially the same hybridization results. The specificity of oligonucleotides was confirmed by a BLAST GenBank search (www.ncbi.nlm.nih.gov) and showed no significant crossmatches with known sequences and expressed sequence tags (ESTs). The oligonucleotides were end-labeled using terminal deoxynucleotide transferase (Boehringer, Germany) and [α-^{35}S]deoxyadenosine triphosphate (dATP) (DuPont NEN, USA), and used for in situ hybridization. Hybridization was performed for 16 h at 42°C in a humidified chamber after which the slides were washed as follows: 2×30 min in 1×SSC at 56°C and 1×10 min in 0.5×SSC at room temperature. Finally, the sections were rinsed in H_2O at room temperature and dehydrated. Slides were exposed to Kodak X-OMAT AR X-ray film for autoradiography for 20 days. Sections hybridized with sense oligonucleotides and sections hybridized with antisense oligonucleotides in the presence of antisense oligonucleotides in 40-fold surplus served as controls. These controls showed only background hybridization signals. After exposure, slides were counterstained with cresyl violet [18].

2.5. Quantitative in situ hybridization analysis

Four animals were analyzed by in situ hybridization for each post-lesion time point and the unlesioned control values. For each animal, two in situ hybridization autoradiographs of adjacent brain slices were used to quantify signal strength. The quantification was performed as described [18]. In brief, for analysis of these images, a computerized videodensitometry system (Metamorph Universal Imaging Inc. West-Chester, PA, USA) was used to quantify the signal intensity on a 600×600 dpi resolution. A visually established pixel intensity threshold was set to remove the unlabeled portion of the image. A rectangle (1.5 mm^2) was defined and placed in 10 different positions over the lesion site (brain parenchyma). For each position, the percentage of pixels within the rectangle representing signal intensities higher than the threshold was determined; signal intensities above this value were not further discriminated. Gray scale values between 0 and 255 were assigned to the grayness of autoradiographic images, the background (less than 20 gray scale values) was subtracted, and the corresponding relative optical density was determined. Data were corrected for film background and expressed in relative optical density. A mean value of the 10 measurements was calculated for each region and set in reference to the unlesioned controls (100%). Analysis was performed using the Mann–Whitney *U*-test. The level of significance was set at $P < 0.05$ (Statview II, Abacus, Berkeley, CA, USA).

2.6. Cell culture and subcellular localization

COS-7 cells (ATCC: CRL-1651) and BV-2 microglial cells (kindly provided by Dr. V. Bocchini, University of Perugia, Italy) were routinely maintained at 37°C with 5% CO_2 in Dulbecco's modified Eagle's medium supplemented with 10% fetal bovine serum, 100 U/ml penicillin, and 100 μg/ml streptomycin as described [19]. Isolation and culture of primary neurons was performed as described [20]. Transfections with the pMAF-eGFP and peGFP-N1 (BD Clontech, Heidelberg, Germany) constructs were performed by Amaxa Nucleofector electroporation (Amaxa Biosystems, Köln, Germany) revealing nearly

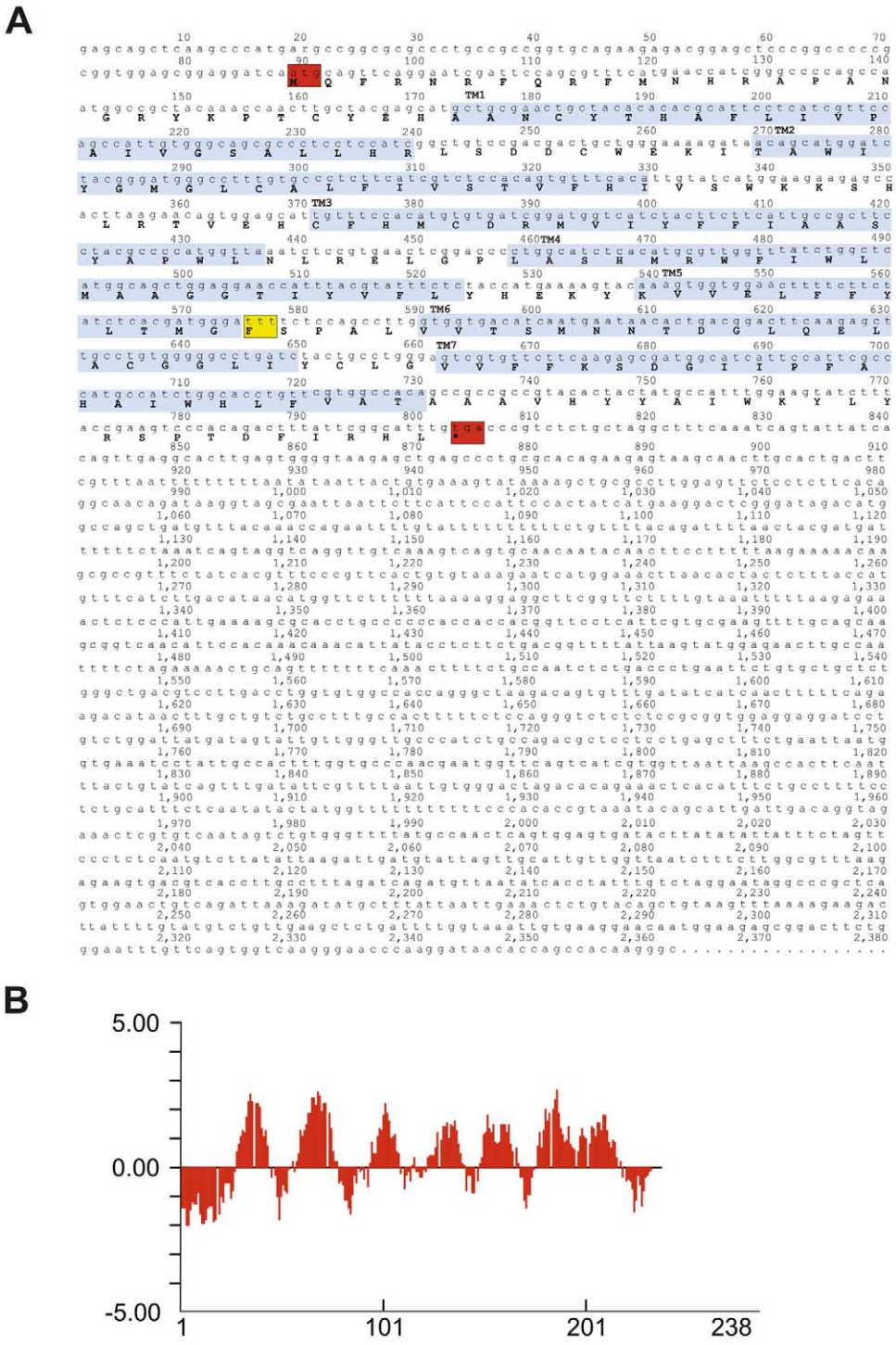

Fig. 1. MAF nucleotide and amino acid sequence. A: Rat MAF nucleotide and amino acid sequence (GenBank accession number AF540876). The putative transmembrane domains (TM1–TM7) are boxed in blue. Start and stop codons are marked in red boxes. The putative glycosylation site is boxed in yellow. B: Hydrophobicity profile of MAF predicted by Kyte–Doolittle algorithms and a window size of five residues. Numbers in the bottom refer to amino acid residues from the amino-terminus.

90% green fluorescent cells. Hoechst staining was performed according to the protocol by Brauer et al. [19]. Images were taken with a CCD camera on a Leica DM LB microscope. Digital data were processed with MetaVue 4.62 software. All constructs were validated by DNA sequencing prior transfection experiments (Dr. S. Prehn, Center for Biochemistry, Charité University Medical School, Berlin, Germany). Cell viability was measured with the MTT assay and nuclear factor (NF)-κB translocation was assayed via immunoblots from nuclear fractions [20].

2.7. Lysosomal staining and immunofluorescence

COS-7 cells and BV-2 microglial cells were fixed with 4% paraformaldehyde in phosphate buffer (150 mM NaCl, pH 7.4) for at least 30 min, quenched by 5 min incubation in 50 mM NH_4Cl, and permeabilized with phosphate buffer containing 0.1% Triton X-100 (Merck, Germany) for 10 min. Lamp-1 antibody (Developmental Studies Hybridoma Bank, Iowa City, IA, USA) was incubated for 6 h at 4°C, washed three times for 10 min, and incubated with an IgG immune-absorbed Alexa 568™ antibody (Molecular Probes) for

1 h at room temperature. LysoTracker™ staining was performed according to the manufacturer's instructions (Molecular Probes, Eugene, OR, USA). Specimens were processed for immunofluorescence microscopy, mounted on Immu-Mount (Thermo-Shandon, Pittsburgh, PA, USA) and viewed on a Leica DM LB microscope. All images were taken with a standardized exposure protocol: $t_{exp} = 5.25$ s for GFP channel; $t_{exp} = 3.20$ s for tetrarhodamine isothiocyanate (TRITC) channel; $t_{exp} = 0.12$ s for HOECHST. Quantification of number and size of late endosomes/lysosomes and vesicles was performed with the MetaMorph analysis system (Universal Imaging, PA, USA). Precise measurements of distances of endosomes/lysosomes from the nucleus were performed in three independent experiments for each cell line with $n = 20$ per experiment. For statistical analysis Statview II was used (Abacus, USA).

3. Results

3.1. Identification of MAF

By DDRT-PCR screening of randomly amplified cDNAs from lesioned and non-lesioned control rat hippocampi, we identified a 1240 bp fragment with high homology to EST clones coding for hemolysin-like genes in vertebrates and prokaryotes. Full-length cloning from brain cDNAs revealed a single 2563 bp product which was directly T/A cloned. After insert size analysis, this clone was subjected to sequencing and the orthologue was revealed to be an uncharacterized human macrophage-specific cDNA [21] (GenBank accession number AF540876) (Fig. 1A). Computer structural analysis (HMMTOP, PREDICT PROTEIN, TMHMM, TMPRED) consistently predicted that MAF cDNA encodes for a membrane protein with seven transmembrane domains. In silico GenBank searches revealed further that these hydrophobic domains are highly conserved in the animal kingdom, from bacteria to humans. GenBank searches for orthologous proteins show that the MAF is highly conserved in mammals (human/mouse/rat $>95\%$), and partial EST sequences indicate orthologous proteins in bacteria, *Caenorhabditis elegans*, *Drosophila* and in other invertebrate genomes as well. This gene encodes

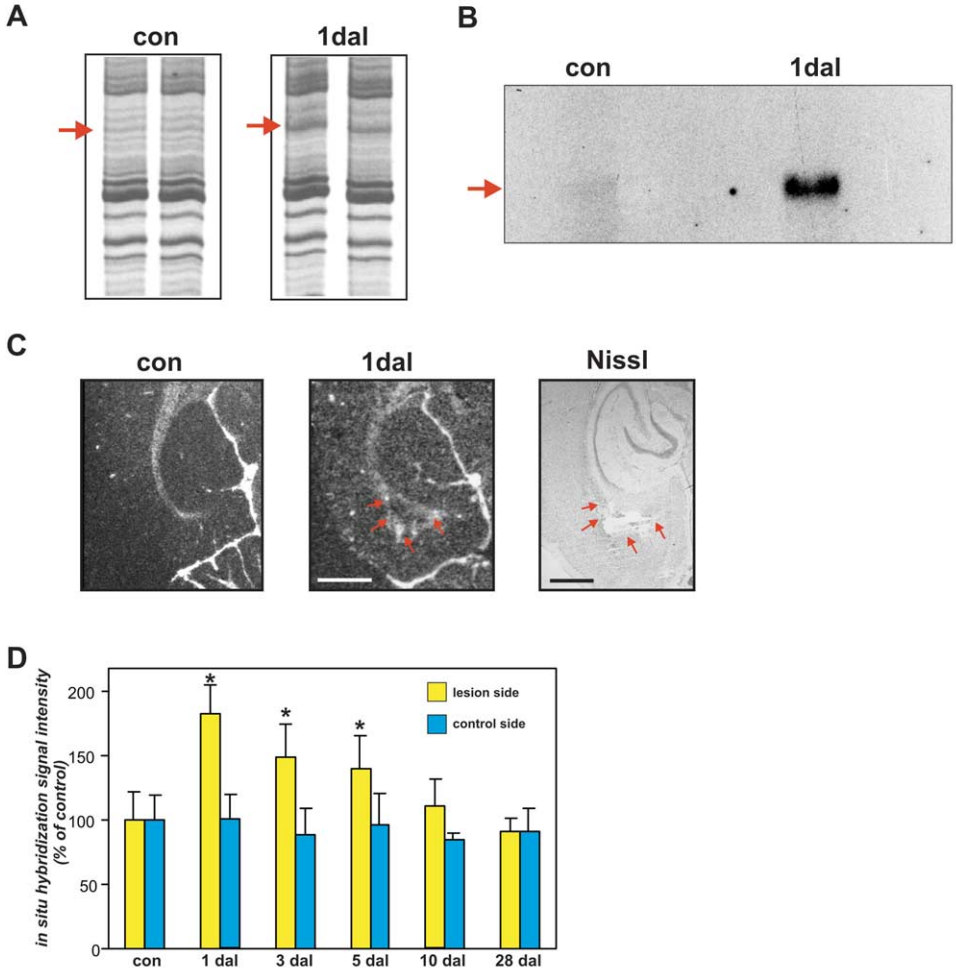

Fig. 2. MAF is upregulated following brain lesion. A: MAF mRNA upregulation following lesion. Differential display mRNA analysis was carried out with 2 μg total RNA of deafferentiated hippocampi 1 dal and non-lesioned control hippocampi (con). One PCR product representing the MAF fragment shows a stronger band in the lanes of lesioned hippocampi versus lanes with the control hippocampi (red arrows). B: Northern blot analysis of MAF transcripts in non-lesioned controls and lesioned hippocampi (1 dal). A strong upregulation of MAF mRNA following lesion is shown (black arrow). C: MAF mRNA expression in the adult non-lesioned hippocampus (con) and in the lesioned hippocampus (dal). Red arrows indicate the increased expression in brain parenchyma following lesion. Right image shows a consecutive brain section (1 dal) stained with cresyl violet (Nissl). Arrows indicate areas of increased MAF mRNA expression. Scale bars represent 1.8 mm. D: Quantitative analysis of MAF mRNA expression in the hippocampus following lesion. For each lesion stage, three animals received an ECL and were killed at 1, 3, 5, 10, and 28 dal. Data are expressed as percentage values compared to non-lesioned controls. Error bars indicate ±S.D. Statistical significance is marked with an asterisk ($P < 0.05$; Mann–Whitney U-test).

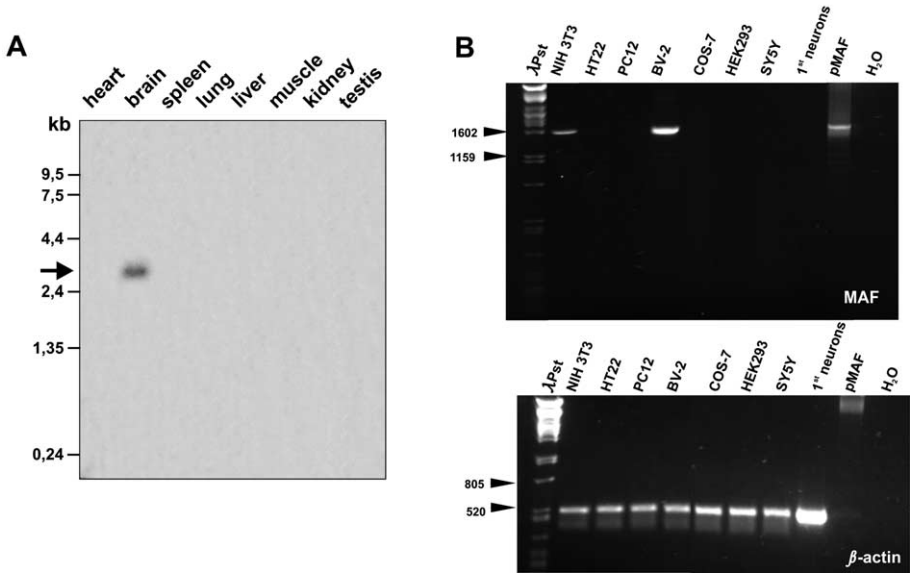

Fig. 3. Tissue distribution of MAF transcripts. A: Multi-tissue Northern blot analysis of MAF mRNA shows a single 2.6 kb band in the brain. B: RT-PCR from NIH 3T3, HT22, PC12, BV-2, COS-7, HEK293, SH-SY5Y, primary (1st) neurons, and pMAF vector (10 ng) serving as a positive control. Arrowheads indicate the reference size from the *Pst*I-digested λ phage. β-actin RT-PCR indicates equal cDNA quality.

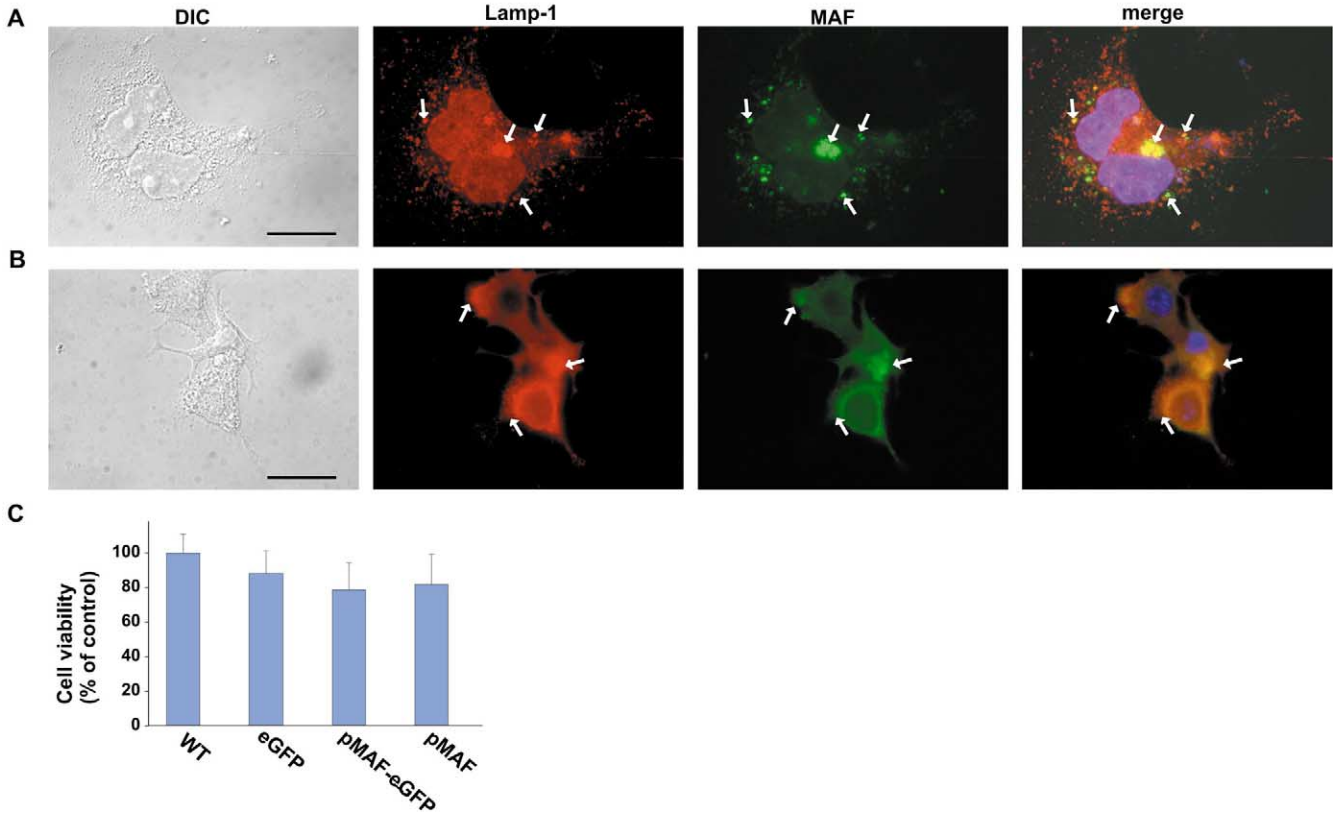

Fig. 4. MAF is associated with endosomes/lysosomes in COS-7 and microglial cells. Overexpression of eGFP-tagged MAF (green) in COS-7 cells (A) and BV-2 microglial cells (B) and subsequent immunohistochemical analysis reveal colocalization with a marker of late endosomes and endosomes/lysosomes, lamp-1 (red). Differential interference contrast (DIC) images show healthy COS-7 cells. MAF is localized in cytoplasmatic vesicles, which are colocalized with the lysosomal marker lamp-1 (arrows). Note that the organization of MAF-associated vesicles appears more dynamic as their size exhibits greater heterogeneity (0.2–3 μm). They are dispersed from the nucleus and border the plasma membrane. Scale bars in A: 25 μm; in B: 9 μm. C: Cell viability of COS-7 cells 24 h after transfection. Note that MAF overexpression did not significantly affect cell viability. Error bars indicate ±S.D.

an as yet uncharacterized membrane protein with seven putative hydrophobic domains (Fig. 1B).

RT-PCR and Northern blot analysis revealed one distinct band of 2.6 kb size in lesioned hippocampi, whereas only weak hybridization signals appeared in the lanes of non-lesioned control hippocampus (Fig. 2A, B).

In situ hybridization analysis highlighted lesion-induced regulation of MAF specifically in the denervated area of the hippocampus (Fig. 2C, D). This lesion-induced MAF upregulation was restricted to the affected area, whereas non-affected brain areas did not show any altered expression (Fig. 2C, D). We further investigated the tissue distribution of MAF mRNA and found predominantly brain tissue as a source of MAF expression (Fig. 3A). Since brain tissue contains primarily neuronal and glial cells, we further elucidated the source of MAF expression. RT-PCR analysis revealed MAF expression mainly in microglial cells (BV-2), whereas neuronal cells were devoid of MAF expression (primary neurons, HT22, PC12, SH-SY5Y) (Fig. 3B). Furthermore, at least one cell line which does not originate from the monocyte/macrophage hemapoetic line (NIH 3T3 cells) also expresses MAF (Fig. 3B).

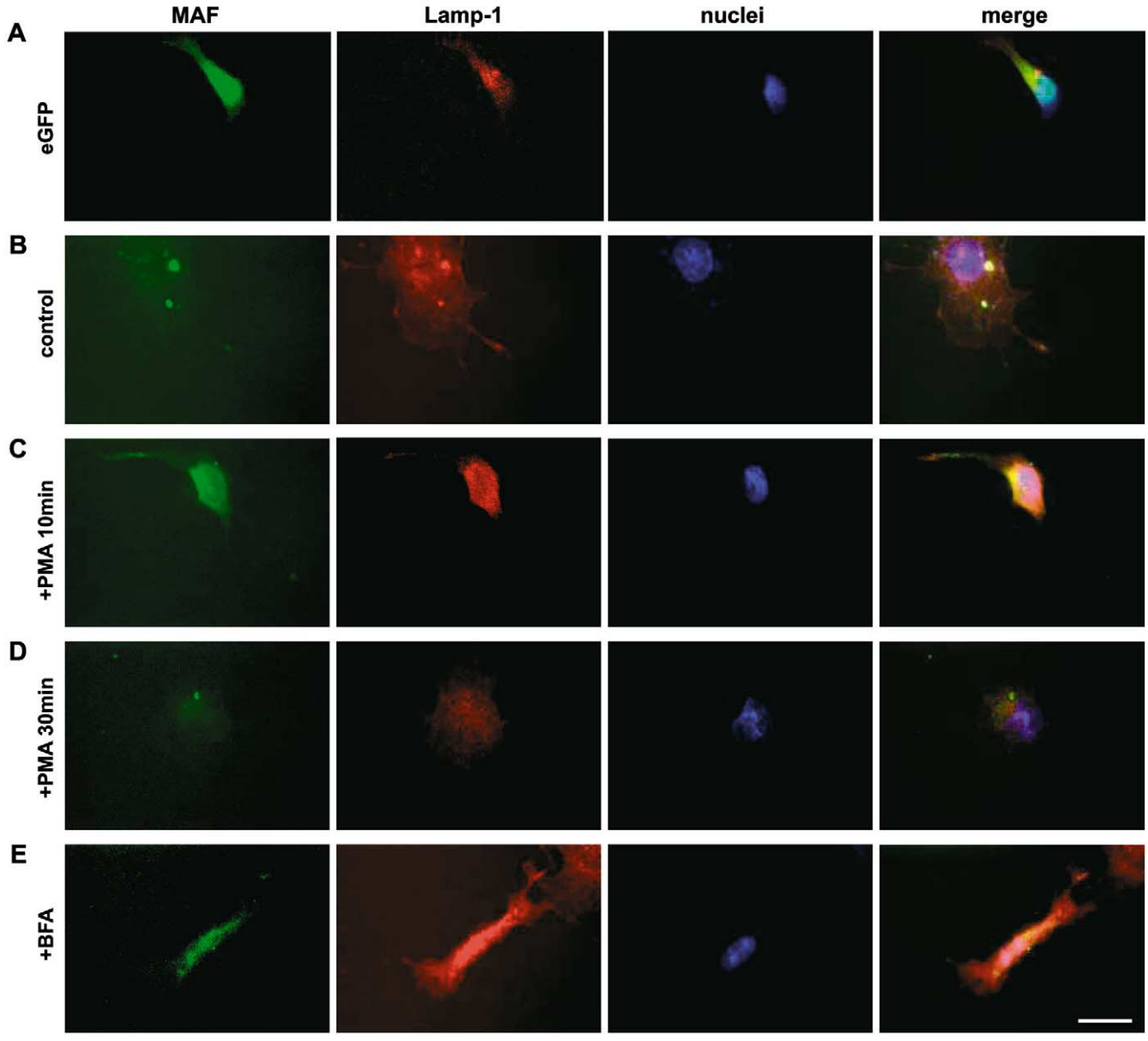

Fig. 5. MAF secretion is mediated in a PKC-dependent manner. A: Distribution of eGFP in COS-7 cells. Note that eGFP is homogeneously distributed throughout the cytoplasm and does not codistribute to lamp-1 positive vesicles. B: Distribution of eGFP-tagged MAF in COS-7 cells. In transfected cells MAF was typically detected in small (0.2–1.0 μm) cytoplasmic, vesicular-like structures located in the cytoplasmatic periphery (green). All MAF positive vesicles show colocalization with lamp-1 (red). C and D: Treatment of COS-7 cells with PMA, an enhancer of exocytosis, for 10 and 30 min. 10 min after PMA treatment, MAF/lamp-1 positive vesicles show a wide and increased distribution throughout the cytoplasmatic periphery. 30 min after PMA application almost all MAF vesicles vanished. E: COS-7 cells treated with BFA, a blocker for the traffic of secretory proteins from the ER to the Golgi complex. Note the accumulation of lamp-1 positive as well as MAF-associated vesicles in the cytoplasm. Scale bar represents 15 μm.

3.2. MAF is associated with mature endosomes/lysosomes

To gain some insight into the subcellular distribution and possible function of MAF, we constructed vectors bearing the wild-type MAF and MAF tagged with an eGFP. Cells were transfected by a modified electroporation method and subsequently immunostained with anti-lamp-1 antibody. In COS-7 and microglial cells, MAF appeared concentrated in vesicular structures densely scattered in the cell body mainly juxtanuclearly and underneath the plasma membrane (Fig. 4A, B). Occasionally, MAF was localized in some larger juxtanuclear vesicular structures and in diffuse, fine, punctate cytoplasmic structures in addition to vesicles, whereas MAF was not present in the nucleus (Fig. 4B). Both eGFP fusion to MAF at the N-terminus as well as eGFP tag at the C-terminus gave essentially the same subcellular distribution (data not shown). The organization of the MAF-associated vesicular structures exhibited great heterogeneity, as their size ranged from 0.2 μm up to 3 μm (Table 1).

Next we analyzed the nature of the MAF positive vesicular structures. Given their peripheral distribution and round shape we hypothesized that these structures are of endocytic origin: endosomes, recycled endosomes or late endosomes/lysosomes [22]. To test this we performed double staining using markers for mature or secondary endosomes/lysosomes [23]. Indeed, using the marker lamp-1, we were able to demonstrate that the MAF-associated vesicles are lamp-1 positive (Fig. 4A, B). In transfected cells, cytoplasmic MAF labeling and anti-lamp-1 staining were coincident. Nearly all MAF positive vesicles were positive for lamp-1 but some lamp positive endosomes/lysosomes were not labeled for MAF. To confirm the lysosomal localization and to exclude possible artefacts and mistargeting due to overexpression, we used:

(i) transfection with a vector solely bearing the reporter gene eGFP,

(ii) microglial cells, which endogenously express MAF.

Transfection with the wild-type MAF-bearing vector or with eGFP-tagged MAF did not affect cell viability or stress-induced NF-κB activation (Fig. 4C). Transfection experiments in BV-2 microglial cells confirmed that MAF is specifically localized in late endosomal/lysosomal compartments (Fig. 4B, Table 1). Controls expressing solely eGFP showed a distinct subcellular organization to MAF, with a homogeneous distribution throughout the cytoplasm unrelated to lamp-1 positive vesicles (Fig. 5A).

3.3. MAF is excreted in a PKC-dependent manner

In order to analyze the functional association of MAF with endosomes/lysosomes, and to demonstrate that MAF overexpression does not artificially affect intracellular processing and cell function, we decided to take a pharmacological approach to lysosomal secretion. COS-7 and microglial cells were therefore treated with phorbol-12 myristate-13 acetate (PMA), a strong PKC activator, and endosomes/lysosomes were monitored (Fig. 5B–D). 10 min after PMA treatment, MAF/lamp-1 positive vesicles showed a wide distribution throughout the cytoplasmatic periphery (Fig. 5C). 30 min after PMA application, most of the lamp-1 positive vesicles disappeared (Fig. 5D). To the same extent, MAF positive vesicles vanished after PMA incubation, whereas eGFP expressing controls exhibited no fluorescence change (data not shown). Treatment of COS-7 cells with brefeldin A (BFA), a blocker for the traffic of secretory proteins from the ER to the Golgi complex, revealed an inverse situation. BFA treatment retained MAF and lamp-1 positive vesicles reversibly. In addition, the MAF/lamp-1 colocalized vesicles increased during the course of BFA application (Fig. 5D). Furthermore, MAF-associated vesicles accumulated around the nucleus and in the cytosol and codistributed with the lamp-1 positive compartment (Fig. 5E). Transfection of BV-2 microglial cells revealed the same dynamic distribution of MAF positive vesicles after PMA treatment as found in COS-7 cells (data not shown).

Table 1
MAF-associated vesicles in COS-7 cells and BV-2 microglial cells

Size of lamp-1/MAF immunopositive vesicular structures			
COS-7 cells		BV-2 microglial cells	
Vesicular size in μm	*n*	Vesicular size in μm	*n*
0.2–1.0	36 ± 8	0.2–1.0	29 ± 7
> 1.0–2.0	9 ± 5	> 1.0–2.0	5 ± 3
> 2.0	4 ± 1.9	> 2.0	2 ± 1

All lamp-1 positive MAF containing vesicular-like structures were submitted for counting by two independent observers. Results are means ± S.D. per cell ($n = 20$ per experiment out of three sets of experiments).

4. Discussion

In this study, we describe the identification, expression, regulation and distribution of a new late endosome/lysosome-associated molecule, MAF, which is specifically expressed in microglial cells. MAF is upregulated following ECL during periods characterized by glial activation and neuronal degeneration. Microglial activation has detrimental effects on neuronal survival and connectivity following brain lesion [9]. Once activated, microglial cells transform into an ameboid-like phenotype [13] and migrate towards the lesion site [12,24], where they secrete inflammatory and cytotoxic molecules, such as tumor necrosis factor (TNF)-α and interleukin (IL)-1β [14,25], phagocytose neuronal debris, and sublethally damaged neurons [9,26,27]. The combination of these processes leads to secondary brain damage, accounting for most of the volume of damaged brain area and loss of brain function [2]. The expression and activation of lysosomal enzymes commence prior to the onset of neuronal apoptosis and cell death, indicating that microglia are actively involved in this process [9,28,29]. Blockage of microglial activation following brain damage has beneficial effects on neuronal outcomes, such as survival, dendritic and axonal morphology, and regenerative axon growth [14,30]. Specifically, interference with the lysosomal pathway in microglial cells can prevent secondary neuronal damage [2,14]. By means of DDRT-PCR from lesioned brain tissue, we identified the MAF, a new membrane protein with seven transmembrane domains. Expression analysis revealed that MAF shows a distribution in late endosomes/lysosomes. Consistent with this is a putative *N*-glycosylation site localized at the cytoplasmatic/luminal site of MAF. Furthermore, MAF shows a dynamic intracellular regulation. MAF is primarily associated with late endosomes/lysosomes, and this association can be disrupted by activation of PKC-dependent pathways.

Recently, a new membrane progesterone receptor family (mPR) has been identified in spotted seatrout oocytes [31]. It has been suggested that these molecules encode plasma membrane proteins with seven putative transmembrane do-

mains. Multiple sequence alignments revealed that MAF shows 71% homology to mPR10 and almost 99% identity to mPR11. So far, the exact cellular distribution of mPR10 and mPR11 has not been proven. Our results indicate that MAF is associated with late endosomes/lysosomes. However, the exact function of MAF remains to be established. It is conceivable that MAF acts as a receptor or sensor on late endosomes/lysosomes, but we cannot yet exclude the possibility that MAF also acts as an anchoring scaffold or modulator and regulator of membrane transport towards lysosomal compartments and secretion. On the other hand, it is also possible that MAF is targeted to the plasma membrane and acts as a sensor for chemotaxis, since lysosomes are able to fuse with the surface plasma membrane [32].

In conclusion, these results imply that MAF is involved in the dynamics of late endosomal/lysosomal membranes of microglial cells. Moreover, MAF is expressed by activated microglial cells, which may contribute to the secondary neuronal degeneration following brain lesion. Thus, future studies using gene silencing approaches (siRNA techniques or genetic disruption strategies) will provide further insights into the role of MAF during microglial–neuronal interactions.

Acknowledgements: The authors thank Bettina Brokowski and Tobias Thiele for their expert technical support; and Sabine Lewandowski for her help with digital image processing. Further, we thank Siegfried Prehn and Elke Bürger (Center for Biochemistry Berlin) for their expert help throughout the course of molecular cloning and sequencing, and subcellular analysis. Andrew Mason is gratefully acknowledged for editorial assistance and helpful suggestions on the manuscript. This study was supported by the Deutsche Forschungsgemeinschaft (DFG): SFB 515/A5. N.E. Savaskan is an Investigator of the Charité Medical Research Foundation.

References

[1] Lynch, G., Stanfield, B., Parks, T. and Cotman, C.W. (1974) Brain Res. 69, 1–11.
[2] Brown, D.R., Schmidt, B. and Kretzschmar, H.A. (1996) Nature 380, 345–347.
[3] Frotscher, M., Heimrich, B. and Deller, T. (1997) Trends Neurosci. 20, 218–223.
[4] Merrill, J.E. and Benveniste, E.N. (1996) Trends Neurosci. 19, 331–338.
[5] Savaskan, N.E. and Nitsch, R. (2001) Rev. Neurosci. 12, 195–215.
[6] Braak, H., Braak, E. and Bohl, J. (1993) Eur. Neurol. 33, 403–408.
[7] Hyman, B.T., Flory, J.E., Arnold, S.E., Van Hoesen, G.W., Schelper, R.L., Ghanbari, H. and Haigler, H. (1991) J. Geriatr. Psychiatry Neurol. 4, 231–235.
[8] Van Hoesen, G.W., Hyman, B.T. and Damasio, A.R. (1991) Hippocampus 1, 1–8.
[9] Cataldo, A.M., Hamilton, D.J. and Nixon, R.A. (1994) Brain Res. 640, 68–80.
[10] Kreutzberg, G.W. (1996) Trends Neurosci. 19, 312–318.
[11] Wood, P.L. (1995) Neurol. Res. 17, 242–248.
[12] Stoll, G., Jander, S. and Schroeter, M. (1998) Prog. Neurobiol. 56, 149–171.
[13] Giulian, D., Chen, J., Ingeman, J.E., George, J.K. and Noponen, M. (1989) J. Neurosci. 9, 4416–4429.
[14] Eyupoglu, I.Y., Bechmann, I. and Nitsch, R. (2003) FASEB J. 17, 1110–1111.
[15] Brauer, A.U., Savaskan, N.E., Plaschke, M., Ninnemann, O. and Nitsch, R. (2003) Neuroscience 121, 111–121.
[16] Paxinos, G., Watson, C., Pennisi, M. and Topple, A. (1985) J. Neurosci. Methods 13, 139–143.
[17] Chomczynski, P. and Sacchi, N. (1987) Anal. Biochem. 162, 156–159.
[18] Brauer, A.U., Savaskan, N.E., Plaschke, M., Ninnemann, O. and Nitsch, R. (2001) Neuroscience 102, 515–526.
[19] Brauer, A.U., Savaskan, N.E., Kuhn, H., Prehn, S., Ninnemann, O. and Nitsch, R. (2003) Nat. Neurosci. 6, 572–578.
[20] Savaskan, N.E., Brauer, A.U., Kuhbacher, M., Eyupoglu, I.Y., Kyriakopoulos, A., Ninnemann, O., Behne, D. and Nitsch, R. (2003) FASEB J. 15, 112–114.
[21] Rehli, M., Krause, S.W., Schwarzfischer, L., Kreutz, M. and Andreesen, R. (1995) Biochem. Biophys. Res. Commun. 217, 661–667.
[22] Oda, K. and Nishimura, Y. (1989) Biochem. Biophys. Res. Commun. 163, 220–225.
[23] Griffiths, G., Hoflack, B., Simons, K., Mellman, I. and Kornfeld, S. (1988) Cell 52, 329–341.
[24] Heppner, F.L., Skutella, T., Hailer, N.P., Haas, D. and Nitsch, R. (1998) Eur. J. Neurosci. 10, 3284–3290.
[25] Bhat, R.V., DiRocco, R., Marcy, V.R., Flood, D.G., Zhu, Y., Dobrzanski, P., Siman, R., Scott, R., Contreras, P.C. and Miller, M. (1996) J. Neurosci. 16, 4146–4154.
[26] Beyer, M., Gimsa, U., Eyupoglu, I.Y., Hailer, N.P. and Nitsch, R. (2000) Glia 31, 262–266.
[27] Adamchik, Y., Frantseva, M.V., Weisspapir, M., Carlen, P.L. and Perez Velazquez, J.L. Brain Res, (2000) Brain Res. Protoc. 5, 153–158.
[28] Muhleisen, H., Gehrmann, J. and Meyermann, R. (1995) Neuropathol. Appl. Neurobiol. 21, 505–517.
[29] Kopacek, J., Sakaguchi, S., Shigematsu, K., Nishida, N., Atarashi, R., Nakaoke, R., Moriuchi, R., Niwa, M. and Katamine, S. (2000) J. Virol. 74, 411–417.
[30] Tikka, T.M. and Koistinaho, J.E. (2001) J. Immunol. 166, 7527–7533.
[31] Zhu, Y., Bond, J. and Thomas, P. (2003) Proc. Natl. Acad. Sci. USA 100, 2237–2242.
[32] Andrews, N.W. (2000) Trends Cell Biol. 10, 316–321.